Surface Enhanced Raman Scattering (SERS) Based Microfluidics for Single Cell Analysis

Marjorie R. Willner [1], Kay S. McMillan[2], Duncan Graham[3], Peter J. Vikesland*[1], Michele Zagnoni*[2]

[1] Department of Civil and Environmental Engineering and the Institute for Critical Technology and Applied Science Center for Sustainable Nanotechnology (VTSuN), Virginia Tech USA

[2]Centre for Microsystems and Photonics, EEE Dept., University of Strathclyde, Glasgow UK

[3]Centre for Molecular Nanometrology, Department of Pure and Applied Chemistry, WestCHEM, University of Strathclyde, Glasgow UK

*pvikes@vt.edu or michele.zagnoni@strath.ac.uk

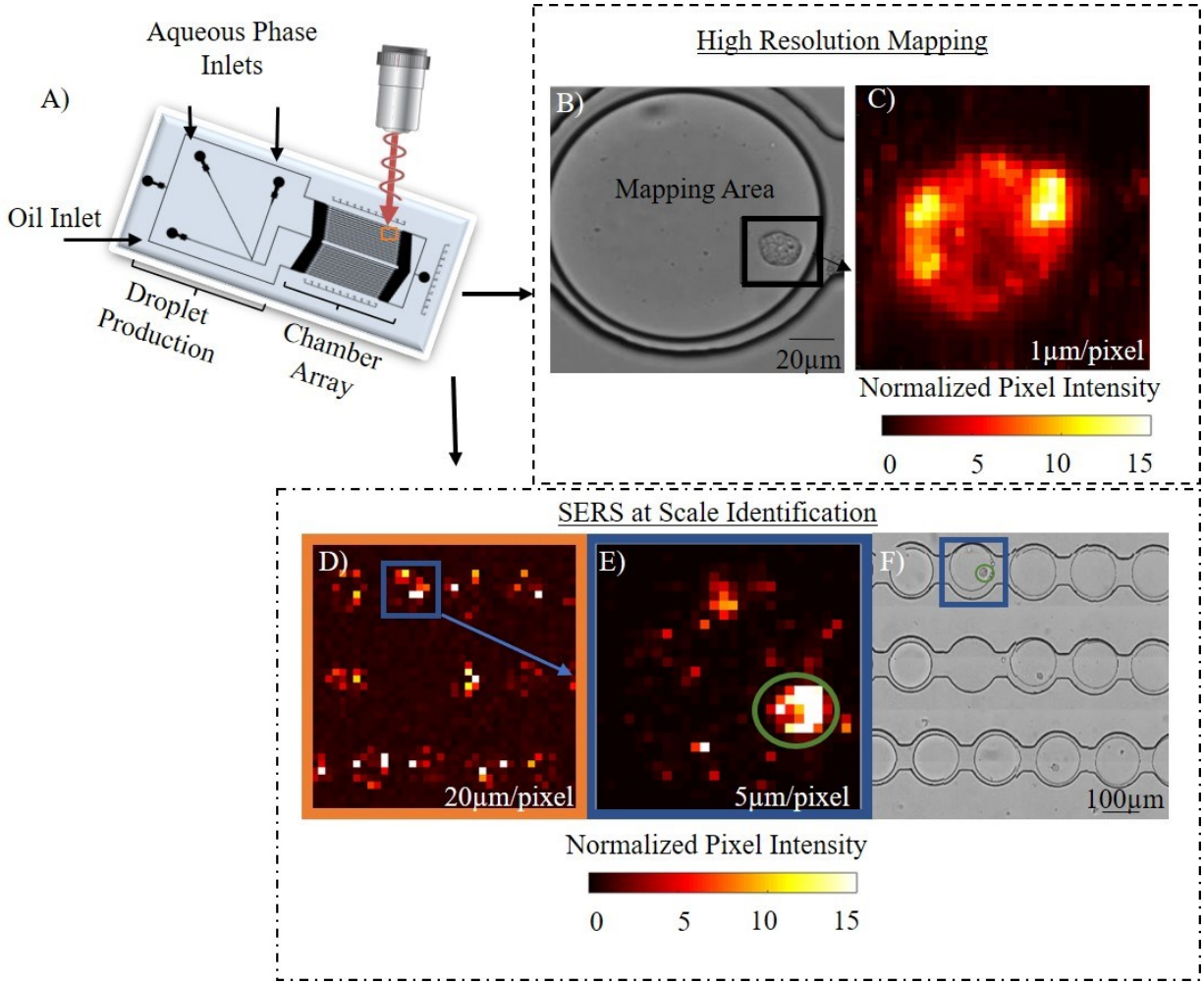

Abstract

The integration of surface enhanced Raman scattering (SERS) with droplet microfluidics has the potential to improve our understanding of cellular systems. Herein, we present the first application of SERS droplet microfluidics for single cell analysis. A microfluidic device was used to encapsulate single prostate cancer cells and wheat germ agglutin (WGA) functionalized SERS nanoprobes in water-in-oil droplets that were subsequently locked into a storage droplet array for spectroscopic investigation. The stationary droplets enabled the rapid identification of SERS regions of interest in live cancer cells by allowing collection of "fast" coarse maps over an area of several mm^2 followed by "slower" detailed interrogation of the identified hotspots. We demonstrate SERS at cellular resolution via a proof-of-concept assay that detects glycan expression on the surface of prostate cancer cells using WGA modified metallic nanoparticles. The data illustrates the potential of SERS optofluidic systems for high-throughput cell screening and illustrates a previously unobserved high degree of cell-to-cell variability in the size and number of glycan islands.

Introduction

Over the past decade, it has become increasingly clear that the genetic and phenotypic characterization of cell populations at the single cell level is a key consideration of fundamental biology research and cell screening. Single-cell droplet microfluidics, combining microfluidic technologies with analytical spectroscopies, presents an exciting opportunity to understand cell-to-cell variability. Significant developments have been made in single-cell -omics[1-3] to the point that digital droplet polymerase chain reaction (ddPCR) instruments are now commercially available. A smaller fraction of the literature has focused on analyzing the behavior of single cells encapsulated in droplets, from metabolite profiling[4] to growth monitoring.[5] Droplet microfluidics enables the production of thousands of individual microreactors in the form of surfactant stabilized emulsions, which are not subject to 'memory effects' or the adhesion of colloid/analyte conjugates within the microfluidic device.[6] The generation of nano- to femto-liter droplets for live cell studies is typically achieved by entraining aqueous droplets in perfluorochemical (PFC) oils that have a very high gas solubility and thus allow for oxygen exchange.[7] Past studies have shown that organisms can be kept alive in droplets for several days.[8]

Surface enhanced Raman scattering (SERS) is a well-established technique that can be used for the detection of trace levels of metals, toxins, pesticides, DNA, proteins, pathogens, and eukaryotic cells.[9-16] SERS is particularly well suited for bioanalytical applications because it is non-destructive and non-invasive and it provides high molecular specificity and spatial resolution.[17] Importantly, fresh tissues and cells can be interrogated with minimal prior preparation because of the weak Raman signal of water molecules.[18] Additionally, SERS has nearly infinite multiplexing capacity and, unlike fluorescence, tag degradation is not a concern.[19] The integration of SERS with droplet microfluidics has been demonstrated for the detection of

crystal violet,[20] potassium ferricyanide,[21] the pharmaceuticals promethazine and mitoxantrone,[22] *Escherichia coli,*[23] *Staphylococcus aureus,*[24] and eukaryotic cell lysate.[25] Using online interrogation (i.e., the collection of SERS spectra from moving droplets), these applications achieved very high-throughput, but collected only one or two spectra per droplet. A benefit of using SERS that was not exploited in these prior studies is the production of high resolution maps. To that end, a different implementation of droplet microfluidics, as popularized by the dropspot device,[26] was used whereby a chamber array was used to keep isolated droplets stationary during SERS interrogation.

In this study, we combine droplet microfluidics with SERS to study cell-to-cell and intracellular variability in the expression of glycans on the cell membrane. Cell membrane carbohydrates are an important oncology target[27] because their overexpression by cancerous cells, relative to healthy cells, can provide an early indication of cancer. Previously, we demonstrated that the glycan N-acetyl neuraminic (sialic) acid expressed by cancerous prostate (PC3) cells can be targeted using the lectin wheat germ agglutinin (WGA).[10] This glycan detection assay was selected for three main reasons: first, the sialic acid residues (target) are abundant on the cell membrane; second, the attachment of the recognition element (lectin) to gold nanoparticles via streptavidin-biotin chemistry is a robust and rapid functionalization method; and, finally, the use of a reporter molecule underscores the potential of this technique to be used for multiplex detection. The use of an established assay allowed us to focus this study on the development of an integrated microfluidic system and the associated analysis algorithms. The two major outcomes of this work are the demonstration of the ability to probe the contents of stationary droplets over a variety of scales and the first application of whole cell imaging using SERS microfluidics.

Materials and Methods

Device Design and Preparation. Microfluidic devices were fabricated using standard photo- and soft-lithography techniques, as previously described.[28] Briefly, master templates with a final resist thickness of 50 μm were produced on silicon wafers using SU8 photoresist (3000 series, MicroChem, US) following the manufacturer's protocol. The resist was exposed through a photomask (JD Photo-Tools, UK) to UV light and was developed in Micro-Posit EC solvent (Rohm and Haas, US). Finally, the wafer surface was silanized by vapor deposition of 1H,1H,2H,2H-perfluorooctyltrichlorosilane (Sigma Aldrich, UK) for 1 hour. Polydimethylsiloxane (PDMS) was poured onto the silicon master at a 10:1 (w:w) ratio of base to curing agent, degassed in a vacuum desiccator chamber, and cured at 80 °C for at least 2 hours. The PDMS devices were then peeled from the mold, cut to the desired size, and holes were punched using 1 mm biopsy punches to obtain inlet and outlet ports. Devices were cleaned and irreversibly bonded to glass microscope slides using oxygen plasma and subsequently treated with undiluted Aquapel (PPG Industries) to obtain fluorophilic microchannel surfaces.

Nanoparticle Synthesis and Functionalization. Sodium citrate (final concentration 3.88 mM) was added to 100 mL of boiling 1 mM tetrachloroauric acid under vigorous mixing conditions. The reaction was allowed to run until the solution color changed to wine red, indicating completion. Gold nanoparticles were functionalized in 5 mL batches and were pH adjusted to circumneutral using 0.1 M potassium carbonate. Next, 2 μM of malachite green isothiocyanate (MGITC), a strong SERS dye with a distinct finger print, was used to pre-aggregate gold colloid. The colloid was coated with 0.1 mg/mL streptavidin, and it was then mixed with 2% BSA to quench further aggregation. After > 30 minutes, the colloid was centrifuged and biotin functionalized wheat germ agglutinin (WGA; Sigma-Aldrich, UK) was added to the nanoparticle pellet at a concentration of 0.17 mg per mL colloid. Following

overnight incubation, the nanoprobes were washed three times with 1% BSA in PBS. The local surface plasmon resonance (LSPR) of the probes was between 530 nm and 533 nm as determined by UV-vis and the particle size (z-average) of the probes in 1% BSA was ~130 nm with a polydispersity index between 0.5 and 0.6 as determined by dynamic light scattering (Malvern Nano-ZS, Malvern, UK).

Cell Preparation. Tumourigenic (PC-3) human prostate epithelial cell lines were cultured in RPMI 1640 Medium supplemented with HEPES, 10% fetal calf serum, 1% penicillin, 1% streptomycin, and 1% fungizone (Gibco, UK). Cells were grown to confluence in an incubator at 37 °C with 5% CO_2 and then harvested with trypsin/EDTA. Solutions containing 10^6 cells/mL were used for microfluidic experiments to favor single cell encapsulation events. The Poisson distribution dictates that in passive cell encapsulation the majority of droplets generated are empty with between 5% to 37% of the droplets containing cells.[29]

Device Loading. Microfluidic devices were connected to 1 mL syringes via polytetrafluoroethylene (PTFE) tubing (Cole Parmer). Syringe pumps were used to vary the fluid flow rates between 0.16 and 0.21 mL/hour to produce droplets of the appropriate size at the T-junction. The continuous phase was FC-40 (3M Company) fluorinated oil with 2 wt% block copolymer fluorosurfactant (designed by the Weitz Group at Harvard and supplied by RAN Biotechnologies, catalogue# 008-FluoroSurfactant, Beverly, MA, USA). The dispersed phase was a solution of phosphate buffered saline (PBS) or phenol-free media containing cells that had been incubated with nanoprobes and subsequently washed.

SERS Spectroscopy. Two different instruments were used to collect data. All glycan island data was collected with an inverted Renishaw InVia system (Renishaw, Wolton-under-Edge, UK) employing a 633 nm wavelength excitation laser, 1200 g/mm grating, 20× objective

(N.A. 0.40) with incident power of 1 mW and a 0.1 second per pixel collection time. SERS at scale data was also collected with the same Renishaw instrument and a WITec Alpha 300R confocal microscope (WITec, Ulm, Germany) in an upright set-up employing a 633 nm wavelength excitation laser and a 300 g/mm. The SERS at scale data was collected at several different magnification and collection times as outlined in the test. The details of the objectives use can be found in Table S1.

SERS Processing. A data processing tool was developed in Matlab to process Raman or SERS spectra in the SPC file format. Briefly, spectra were baseline corrected using an asymmetric least squares baseline correction.[30] A peak or peaks of interest were then specified and the intensity of the peaks was automatically extracted from the dataset. For data collected in a rastering format (maps) the intensity at each point could be plotted to generate SERS maps.

Results and Discussion

To interrogate single cells within polydimethylsiloxane (PDMS) microfluidic devices using SERS, a laser must pass through four media (Fig 1A) before interacting with the sample. Malachite green isothiocyanate (MGITC) was selected as the Raman reporter because its signature peaks at 1614 cm^{-1} and 1364 cm^{-1}, assigned to the phenyl-N + C−C stretching mode and the phenyl-N stretching mode[31], do not overlap with the strong PDMS asymmetric and symmetric C-H stretches at 2965 cm^{-1} and 2903 cm^{-1} respectively[32-34] (Fig 1A). Gold nanoparticles (35 nm) were pre-aggregated with MGITC, coated with streptavidin, mixed with biotinylated wheat germ agglutinin (WGA) and then washed to remove unbound WGA. Adherent PC3 cells were removed from the culture flask to create a cell suspension, incubated with the nanoprobes for 10 minutes, washed to remove unbound nanoprobes and ultimately encapsulated in droplets. The droplets were subsequently stored in a chamber array, a modified

147 version of the dropspot device[26], before the device was transferred for imaging by Raman
148 microscopy.

149 SERS data of biological samples is often acquired by defining a region of interest over
150 which the laser is rastered. At each pixel location a spectrum is collected, from each spectrum the
151 same feature (i.e., wavenumber or wavenumber range) is selected, and the value (i.e., intensity or
152 integrated intensity) of the feature is then plotted on an *x*-*y* grid to generate a SERS map.
153 Commonly, conclusions are drawn by manually inspecting SERS maps, but the use of statistical
154 descriptions and chemometric analyses are becoming a standard part of SERS data analysis.
155 Often these higher order descriptions, such as in our work on intracellular pH[35] detection, are
156 accompanied with re-rendered SERS maps that display complex content. However, variability
157 between maps or the physical clustering of regions of interest (i.e., how many pixels that meet a
158 certain criterion are adjacent to one another) is not taken into account. While not appropriate for
159 all experiments, the study of cell expression, especially as enabled by droplet microfluidics,
160 supports the adoption of automated techniques to detect regions of interest. The imaging
161 processing techniques developed in our data tool allow us to generate SERS maps, to then
162 identify regions of interest within each map, and to then statistically analyze the size and
163 distribution of each region.

164 **Development of Data Processing and Analysis Tool.**

165 A workflow diagram illustrating our data processing algorithm is shown in Figure 2. SERS maps
166 enable visualization of the results of a SERS experiment and are a simplification of the total data
167 collected (i.e., a reduction in data dimensionality). Embedded within each pixel of a SERS map
168 is a full spectrum containing 1015 (Wire 4.2) or 1024 (Project FOUR 4.1) points and a myriad of
169 vibrational information. A typical SERS map obtained for the single cell studies contained 900
170 pixels or a total of 9×10^5 points. Baseline correcting, normalizing, and rendering a SERS map

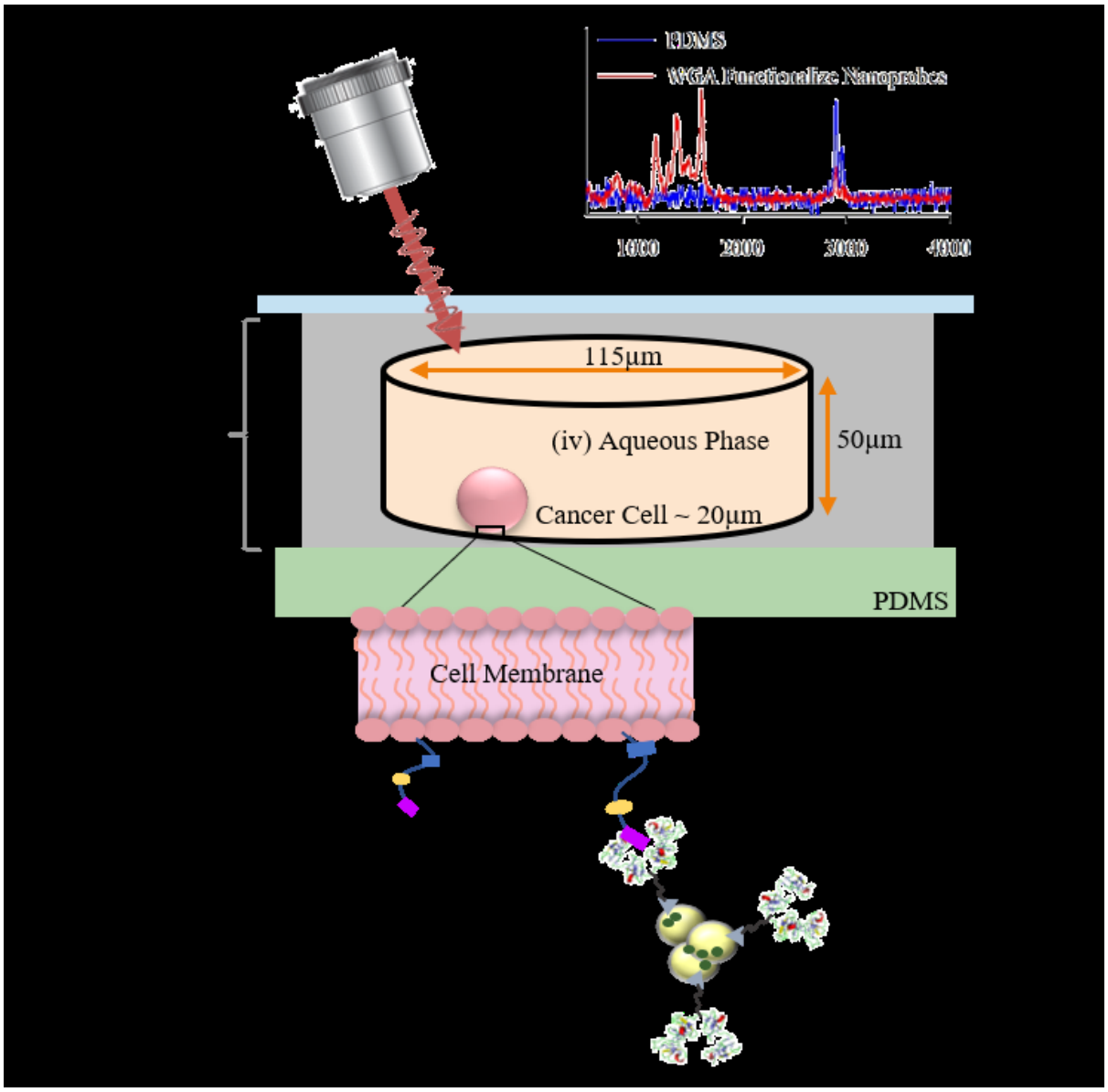

Figure 1. Illustration of a single cell encapsulation event within the microfluidic device. The four media that the laser must pass through before interacting with the target (cancer cell) are labeled from i to iv. The cartoon also includes the dimensions of the microfluidic device and cancer cell. The inset displays the PDMS Raman spectrum through a droplet in the absence of nanoprobes or cells and the SERS spectra from Wheat Germ Agglutinin (WGA) functionalized nanoprobes (A). Zoom in of the cell membrane shows the expression of sialic acid. A WGA functionalized nanoprobe is shown attached to the sialic acid and the individual components of the probe are named (B).

171 based on the intensity of a specific peak can be readily achieved using proprietary software such
172 as Wire 4.2 or Project FOUR 4.1. However, these programs generally lack batch processing
173 capacity, transparency in the data processing algorithms, and the ability to open data files in a

non-proprietary format. To overcome these challenges and to take advantage of the large amount of information available from the SERS optofluidic platform a specialized data analysis and processing tool was written in Matlab. The code is available online at GitHub[36].

To optimize data handling and cross-platform functionality, we exported data from Wire 4.2 or Project Four 4.1 using the SPC file format (.spc). This data was then imported into Matlab for further processing. .spc is preferred over text (.txt) or comma separated value (.csv) files because it contains the raw spectral plus metadata containing additional scan details. Within Matlab, automated baseline correction was achieved using a modification of Eiler's asymmetric least squares baseline estimation.[30] Following normalization, SERS maps could be rendered based on the intensity of a specific peak, the ratio of multiple peaks, or based on the mathematical transformation of a peak ratio.[35] To demonstrate the efficacy of this data processing tool, data from a single experiment was processed using the tool and the Wire 4.2 proprietary software (Fig S2). Collected data was baseline corrected, the intensity of the 1609 cm^{-1} peak was plotted (feature selection) and the maps were scaled using the same look-up-table (LUT) so that they could be directly compared. The resulting maps from the data processing tool and Wire 4.2 were identical. A spectrum to spectrum comparison of the data from a single pixel (Figure S2C & S2D) shows that the baseline corrected data is nearly identical, as would be expected from using distinct algorithms.

The advantages of using this automated tool are evident when processing and analyzing a large number of analyses from an experiment or dataset (i.e., the collection of SERS maps collected from a single microfluidic device). The characteristics of each map, such as the minimum, maximum, and average pixel values, can be collated during processing and can be queried after all the data was processed to define a LUT. The maps can then be rescaled based on

these statistics. For example, in our study of cell-to-cell heterogeneity (discussed *vide infra*) the LUT was defined to be 2× to 3× the standard deviation above the mean. Other variable ranges can be readily defined depending on the desired application. The library of SERS maps were analyzed and edge finding scripts were used to identify regions of interest and the size of clusters meeting certain criteria were calculated.

SERS Whole Cell Imaging and observation of cell-to-cell heterogeneity.

To demonstrate the capacity of the optofluidic platform for single cell analysis, wheat germ agglutin (WGA) was used to target the glycan N-acetyl neuraminic (sialic) acid expressed on cancerous prostate (PC3) cells. Pre-aggregated SERS hotspots coated with WGA – nanoprobes – were mixed, in excess, with PC3 cells, after a ten-minute incubation period the cells were washed to remove unbound nanoprobes and introduced into the microfluidic platform. A Poisson distribution for cell encapsulation in droplets was considered. A cell loading concentration of 10^6 cells per mL favored the formation of single cell encapsulation events.[29] SERS maps were then collected from: i) individual droplets with a focus on single cell encapsulation events, representative images shown in Figure 3A-C; and ii) multiple droplets (discussed in the next section).

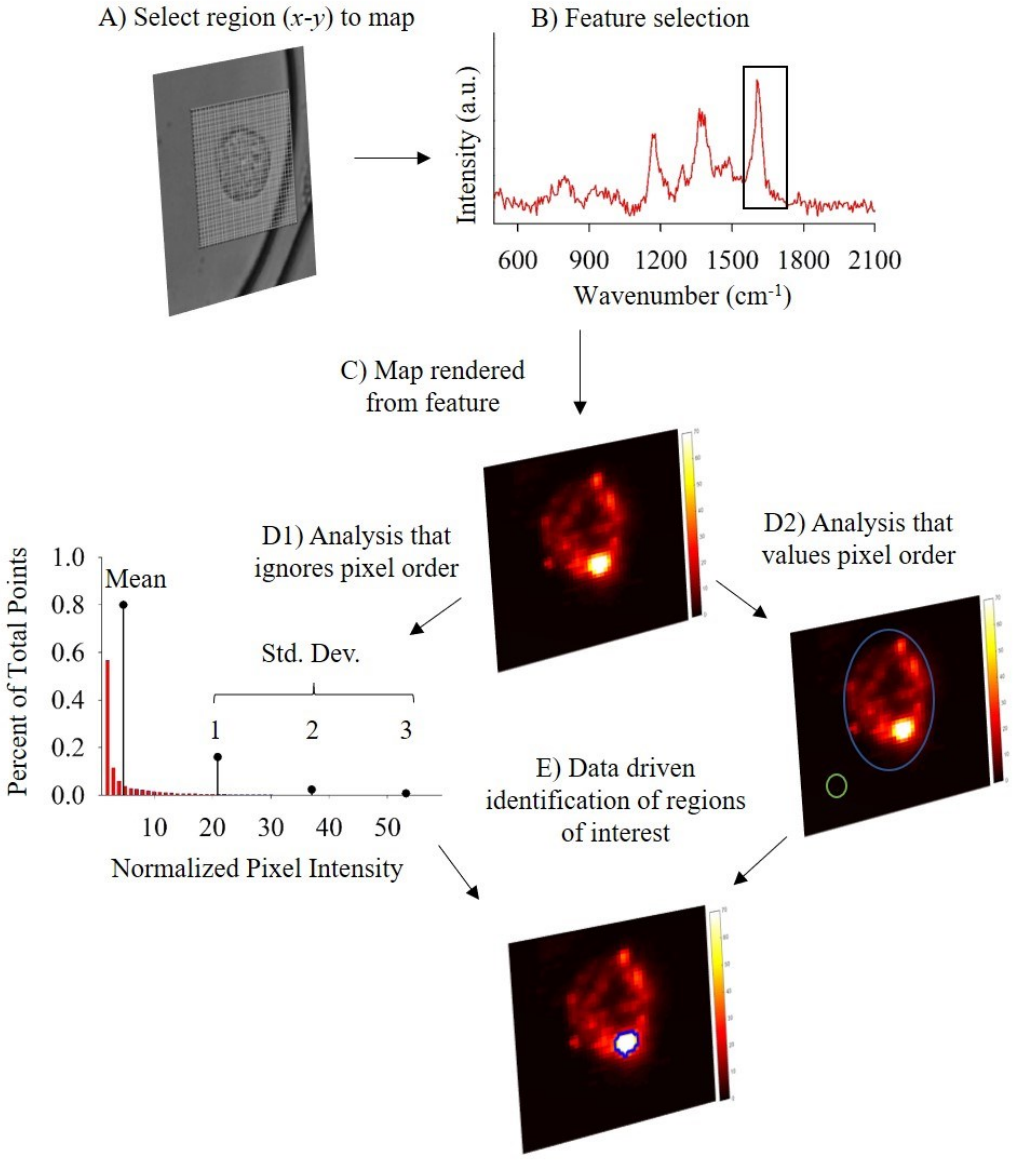

Figure 2. Details of SERS scan: 20× Objective; 40µm by 40µm area of interest; pixel size 1µm/pixel; grating 1200g/mm; 633nm laser; collection time 0.1 seconds. (A) At each pixel a spectrum is collected in two dimensions: intensity vs wavenumber. Pre-processing such as baseline correction and normalization are undertaken followed by feature selection. (B) Single SERS maps are rendered after feature selection to aid in data interpretation. At each *x*-y coordinate the intensity of the feature is depicted using a color (C). A library of maps is generated and increases the dimensionality to 4D (map × *x* location × *y* location × wavenumber) or after feature selection, fixing the wavenumber, 3D (map × *x* location × *y* location). Typical SERS data processing only discusses pixel intensity and uses measures such as mean intensity, standard deviation, etc. to describe the data set. For analysis of cells and other ordered objects crucial information is lost by neglecting pixel order (D1). Corrected total intensity (CTI) is a simple method that values pixel order. The area of interest is selected, blue circle, and the integrated density of the area is calculated (area × mean intensity). From this value, the mean background intensity × area of cell is subtracted to yield the CTI. (D2) Combing the statistical information and pixel order allows for complex analysis of the maps. For example, from the map library (D1) the value of two and three standard deviations above the mean pixel intensity can be calculated. These values can be used to recolor the map (C) and visually the contrast between the background and region of interest (ROI) becomes evident. The data tool can also now distinguish the ROI from the background and determined the size of the ROI (E).

baseline corrected and then normalized by the SERS intensity of the nanoprobes for that experiment. SERS maps, such as those in Figure 3D-F, were generated by selecting the spectral feature at 1609 cm^{-1} and plotting the intensity at each pixel. To compare maps and evaluate cell-to-cell variability, a new parameter, corrected total intensity (CTI), was defined. This parameter, an analogue to corrected total cell fluorescence (CTCF)[37,38], values pixel order and how the object of interest is distinct from the background. A benefit of SERS rastering is the collection of data with four dimensions (*x* location, *y* location, wavenumber, and intensity). In generating a map, the dimensionality of the data is reduced to three dimensions (*x* location, *y* location, and intensity at a specific wavenumber) and allows for intuitive visual inspection that is easily correlated to the mapped feature (i.e., a cell). However, in typical SERS analyses the *x* and *y* mapping data are disregarded and the discussion is focused on the statistical characterization of a spectral feature of interest. While this approach may be appropriate for the mapping of homogenous samples, the study of biological samples demands that the *x*-*y* information, the ordering of the pixels, is taken into account during analysis. Fluorescence spectroscopy often deals with data in the three dimensions of *x* location, *y* location, and intensity and thus we adopted the corrected total cell fluorescence measurement to analyze SERS maps.

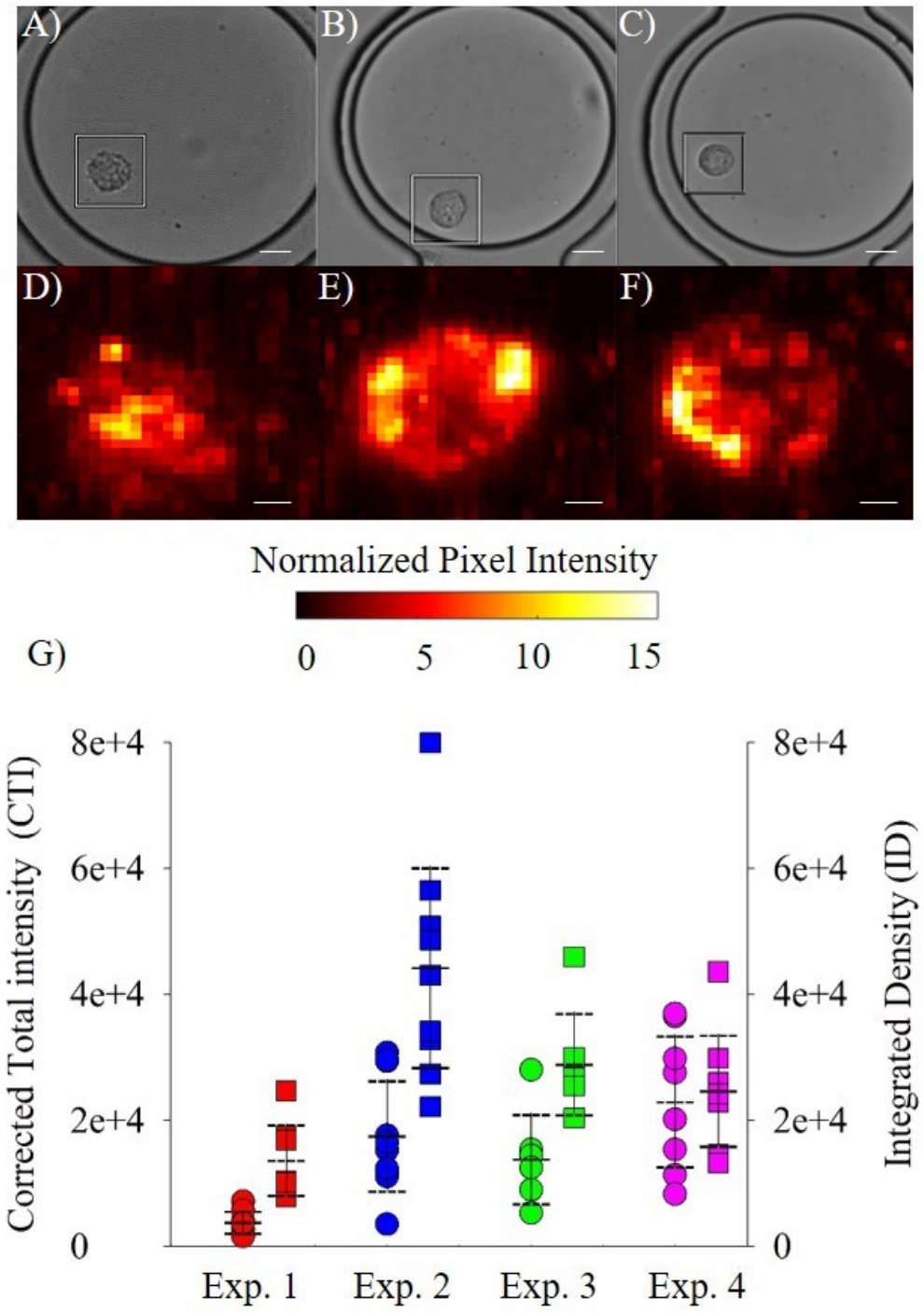

Figure 3. Optical images with a 20μm scale bar (A-C) of single PC3 cells encapsulated in droplets with the corresponding SERS maps with 5μm scale bar (D-F). The corrected total intensity (circles) and integrated dentistry (squares) for four different experiments, each represented in a unique color, with error bars representing one standard deviation (G).

The CTI values were determined by calculating the integrated density, the mean image intensity multiplied by the area of interest, and subtracting the average background intensity. Standard CTCF analysis is performed using ImageJ. Within ImageJ a threshold is applied to an imported image to find the objects of interest and the integrated density is then calculated for those regions of interest. The intensity for the background is then determined in ImageJ and ultimately in Excel (or a program of choice) the CTCF is calculated by finding the difference between the mean intensity in the ROI and the background and multiplying that by the area of the ROI.

Our CTI were calculated in ImageJ using the same protocol except the starting images were SERS maps generated from the data. To demonstrate the need for ROI selection, the CTI data is compared with the total map intensity, the sum of the intensity at every point in the map, or described differently the integrated density of the map without ROI selection Figure 3G.

The coefficient of variation (CoV) was used to describe the variation across the collected data sets and the CTI results had a consistently larger CoV than the total map intensities (SI Table 2). In the total map calculations, the intensity contribution of the cell, which occupies ~30% of the map area, was damped by the background pixels. To demonstrate that the variation in the nanoprobe attachment from to cell-to-cell was neither the product of the functionalization chemistry, nor the orientation of the cells during cell mapping, the experiment was replicated using WGA functionalized with the fluorophore fluorescein (FITC). Interestingly, when the coefficient of variation for the CTFC results were tabulated (SI Table 3) they fell in the same range, 0.4 and 0.6, as the CTI calculations. The results show that there is indeed cell to cell variability in the expression of sialic acid residues on the surface of the PC3 cells.

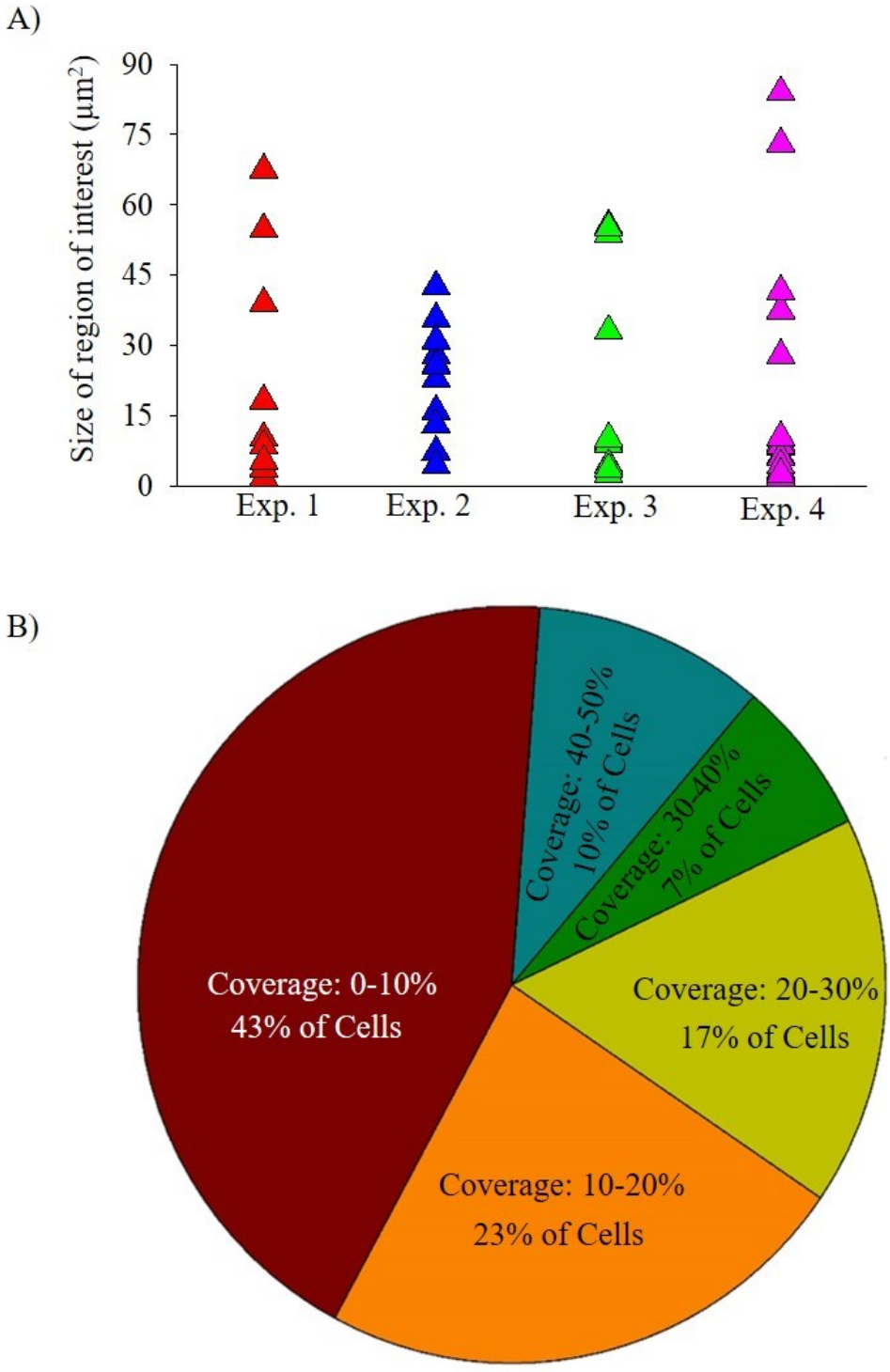

Figure 4. The size of all regions of interest (ROI), classified as a cluster of more than one pixel with an intensity greater than two standard deviations (2×) above the mean, for each experiment (A). Pie graph showing the distribution of ROI size (µm^2) for the whole data set. Each wedge is labeled with the size range and the percentage of ROI in that wedge (B).

In comparing the SERS maps, Figure 3D-F, and the fluorescence images, Figure S3, it was apparent that sialic acid residues were heterogeneously distributed on the cell surface, typically with a large cluster of glycans occurring in one area. To quantify the size of the glycan clusters the data processing tool was expanded for image processing. Specifically, for each experiment the LUT was defined to be 2× to 3× the standard deviation above the mean intensity of the data set; this thresholding set the majority of the background (pixels) to black. Contrast aids the edge finding scripts to determine the boundary between the region of interest and the background. Pixels above the threshold were identified and only clusters containing more than one pixel were extracted from the maps to ensure that the SERS signal was arising from glycan locations and not noise. Furthermore, differences in the probe signal on the cell surface arise most likely from quantitative differences in the sialic acid and not from variation in probe size. Using the work of Haiss et al.[39] to estimate surface plasmon resonance (SPR) of the probes (~135 nm diameter), the majority of the probes will have an SPR at 632 nm, in near perfect resonance with the 633 nm laser. Whereas, the SPR for larger probes will be at higher wavelengths and thus off-resonance and responsible for a smaller fraction of the signal.

Maps could contain more than one cluster. The size of the clusters, in μm^2, was determined and the cluster sizes on a per experiment basis plotted (Figure 4A). Most of the clusters, 53%, were smaller than 10 μm^2 and given that the average PC3 cell is 20 μm in diameter and, modeling the cell simply as a sphere, most clusters cover less than 3% of the cell surface. Even the largest cluster at 84 μm^2 occupies at max 27% of the area of an average cell. However, 47% of cells contain more than one glycan island suggesting that a direct area to area comparison would be more descriptive of glycan expression.

To understand glycan surface coverage in more detail, for each cell the size of the glycan island(s) was compared to the cell area. The exposed cell area was calculated with the same edge finding scripts as the island area except that input figures were the optical images of the cells. The pie graph (Figure 4B) underscores that most of the cells, 66%, had less than 20% of their total exposed area covered by glycans. Returning to the largest cluster, it was found to be the only island on that specific cell, the largest island in the dataset, covered 30% of the area of the cell; extremely close to the initial estimate. The largest total glycan area was 111 μm^2, originating from two islands, and covering 43% of the cell area whereas the cell with greatest coverage, 48%, contained a total glycan area of 74 μm^2. The fact that the largest single island, largest total glycan area, and largest area coverage are found on three different cells underscores that cell-to-cell variability exists and that measuring the differences becomes accessible with the implementation of SERS droplet microfluidics. Moreover, the identification of these heterogeneities on the cell surface prompted biological experiments.

Imaging Across Scales.

A major benefit of using SERS droplet microfluidics is the ability to examine many different cells at once. Typically, as done for whole cell imaging, regions of interest are manually identified under white light and then SERS mapping areas are defined. The process of visually identifying regions of interest is laborious and time consuming especially when compared with fluorescent image collection, such as those in Figure S3, where hundreds of cells can be imaged quickly. Furthermore, the ability to identify SERS ROI's without first using the white light image is advantageous because it removes the reliance on the white light microscope and pushes towards fully automated application. Figure 5 shows the potential of SERS detection at scale with panel B showing a SERS map of a 760 μm by 760 μm region, taken at a relatively low resolution (20μm/pixel). An area of interest was identified and mapped at higher resolution

(5µm/pixel), panel C, and the map clearly showed the presence of a cell. A bright field image was then collected and confirmed the presence of a cell. A more detailed map, such as that in the single cell experiments could also have been easily collected if so desired

SERS at scale presents many exciting capabilities and has the ability to increase the applicability of SERS for biological studies. The ability to survey over 1000 droplets rapidly increases the quantification accessible with SERS for both lab based studies and the production of point-of-care sensors. Rapid SERS screening will allow the method to compete with more

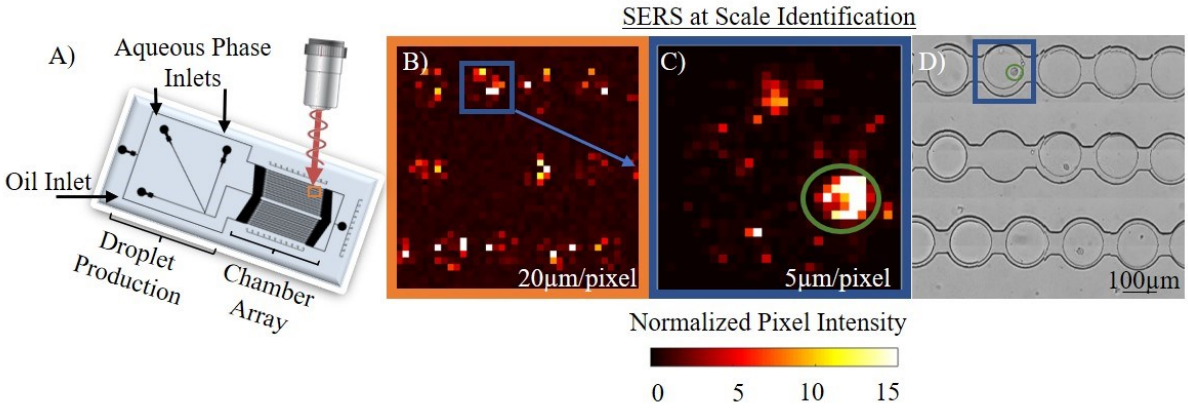

Figure 5. Schematic of the optofluidic platform (A) followed by the SERS at scale process. Note that the orange box in A denotes the SERS mapping shown in B. The processed low-resolution SERS map is shown in B with an area of interested outlined with a blue box. The area of interest is than scanned with higher resolution (C) and a second region of interest, the cell, is circled in green. The white light image of the area, orange box, is collected and then two regions of interest, blue box and green circle, are used to confirm the accurate identification of the cell.

standard techniques such as flow cytometry, but introduce the ability to easily identify and map with high resolution cells of interest. The platform is well suited for the study of environmental samples that are typically sample limited and/or highly dilute. An automated platform will aid in the identification of targets of interest without destroying the sample thus allowing SERS to be combined with more traditional analyses such as culturing or genomics analysis. Another major benefit of using SERS at scale is the ability to study dynamic processes. Unlike, fixed cell

experiments or -omics analyses, the optofluidic platform allows for the study of cellular behavior as a function of time. With slight modifications to the platform, stressors can be introduced into the droplets and SERS can be used to measure changes in the behavior of individual cells, opposed to traditional measurements which look at changes in bulk population behavior.

Conclusion and Future Outlook.

SERS droplet microfluidics is a powerful tool for single-cell analysis and the imaging of aqueous systems of biological importance. In this paper, we have used this technology to show cell-to-cell variation in glycan surface coverage, created a centralized data processing tool and showed the ability to access cellular information at a range of scales. The methods and tools presented herein lay the foundation for future SERS studies and show the first application of the platform for deciphering the composition of cell membranes. Multiplex SERS assays can be deployed in a droplet microfluidic device without any modification to the methods described. Moreover, the use of image processing to interpret SERS maps can be adopted for other applications where the region of interest is only a subset of the total area mapped.

Acknowledgements

This work was supported by US National Science Foundation grants CBET-1133746 and OISE-1545756. Instrumental support was provided by the Virginia Tech National Center for Earth and Environmental Nanotechnology (NNCI - 1542100). Additional support for MRW was provided by the Virginia Tech Graduate School.

Supporting Information

The Supporting Information is available free of charge on the ACS Publications website. Preliminary unprocessed SERS maps, validation of centralized data tool, WGA-FITC tagged

PC3 cells, objectives Used, coefficient of variation for SERS and fluorescence experiments (PDF).

References

(1) Hindson, B. J.; Ness, K. D.; Masquelier, D. A.; Belgrader, P.; Heredia, N. J.; Makarewicz, A. J.; Bright, I. J.; Lucero, M. Y.; Hiddessen, A. L.; Legler, T. C.; Kitano, T. K.; Hodel, M. R.; Petersen, J. F.; Wyatt, P. W.; Steenblock, E. R.; Shah, P. H.; Bousse, L. J.; Troup, C. B.; Mellen, J. C.; Wittmann, D. K., et al. *Analytical chemistry* **2011**, *83*, 8604-8610.

(2) Macosko, E. Z.; Basu, A.; Satija, R.; Nemesh, J.; Shekhar, K.; Goldman, M.; Tirosh, I.; Bialas, A. R.; Kamitaki, N.; Martersteck, E. M.; Trombetta, J. J.; Weitz, D. A.; Sanes, J. R.; Shalek, A. K.; Regev, A.; McCarroll, S. A. *Cell* **2015**, *161*, 1202-1214.

(3) Klein, A. M.; Mazutis, L.; Akartuna, I.; Tallapragada, N.; Veres, A.; Li, V.; Peshkin, L.; Weitz, D. A.; Kirschner, M. W. *Cell* **2015**, *161*, 1187-1201.

(4) Bjork, S. M.; Sjostrom, S. L.; Andersson-Svahn, H.; Joensson, H. N. *Biomicrofluidics* **2015**, *9*, 044128.

(5) Girault, M.; Kim, H.; Arakawa, H.; Matsuura, K.; Odaka, M.; Hattori, A.; Terazono, H.; Yasuda, K. *Scientific reports* **2017**, *7*, 40072.

(6) Theberge, A. B.; Courtois, F.; Schaerli, Y.; Fischlechner, M.; Abell, C.; Hollfelder, F.; Huck, W. T. S. *Angewandte Chemie* **2010**, *49*, 5846-5868.

(7) Lowe, K. C. *J Fluorine Chem* **2002**, *118*, 19-26.

(8) Clausell-Tormos, J.; Lieber, D.; Baret, J. C.; El-Harrak, A.; Miller, O. J.; Frenz, L.; Blouwolff, J.; Humphry, K. J.; Koster, S.; Duan, H.; Holtze, C.; Weitz, D. A.; Griffiths, A. D.; Merten, C. A. *Chemistry & biology* **2008**, *15*, 427-437.

(9) Chung, E.; Lee, J.; Yu, J.; Lee, S.; Kang, J. H.; Chung, I. Y.; Choo, J. *Biosensors and Bioelectronics* **2014**, *60*, 358-365.

(10) Craig, D.; McAughtrie, S.; Simpson, J.; McCraw, C.; Faulds, K.; Graham, D. *Analytical chemistry* **2014**, *86*, 4775-4782.

(11) Lee, S.; Chon, H.; Lee, J.; Ko, J.; Chung, B. H.; Lim, D. W.; Choo, J. *Biosensors and Bioelectronics* **2014**, *51*, 238-243.

(12) Lee, S.; Chon, H.; Lee, M.; Choo, J.; Shin, S. Y.; Lee, Y. H.; Rhyu, I. J.; Son, S. W.; Oh, C. H. *Biosensors and Bioelectronics* **2009**, *24*, 2260-2263.

(13) Pallaoro, A.; Braun, G.; Moskovits, M. *MRS Proceedings* **2012**, *1468*.

(14) Qian, X.; Peng, X. H.; Ansari, D. O.; Yin-Goen, Q.; Chen, G. Z.; Shin, D. M.; Yang, L.; Young, A. N.; Wang, M. D.; Nie, S. *Nature biotechnology* **2008**, *26*, 83-90.

(15) Scaffidi, J. P.; Gregas, M. K.; Seewaldt, V.; Vo-Dinh, T. *Analytical and bioanalytical chemistry* **2009**, *393*, 1135-1141.

(16) Gracie, K.; Correa, E.; Mabbott, S.; Dougan, J. A.; Graham, D.; Goodacre, R.; Faulds, K. *Chemical Science* **2014**, *5*, 1030-1040.

(17) Brautigam, K.; Bocklitz, T.; Silge, A.; Dierker, C.; Ossig, R.; Schnekenburger, J.; Cialla, D.; Rosch, P.; Popp, J. *Journal of Molecular Structure* **2014**, *1073*, 44-50.

(18) Old, O. J.; Fullwood, L. M.; Scott, R.; Lloyd, G. R.; Almond, L. M.; Shepherd, N. A.; Stone, N.; Barr, H.; Kendall, C. *Analytical Methods* **2014**, *6*, 3901-3917.

(19) Laing, S.; Gracie, K.; Faulds, K. *Chemical Society reviews* **2016**.

(20) Liu, B. X.; Jiang, W.; Wang, H. T.; Yang, X. H.; Zhang, S. J.; Yuan, Y. F.; Wu, T.; Du, Y. P. *Microchimica Acta* **2013**, *180*, 997-1004.

(21) Cristobal, G.; Arbouet, L.; Sarrazin, F.; Talaga, D.; Bruneel, J. L.; Joanicot, M.; Servant, L. *Lab on a chip* **2006**, *6*, 1140-1146.

(22) Ackermann, K. R.; Henkel, T.; Popp, J. *Chemphyschem : a European journal of chemical physics and physical chemistry* **2007**, *8*, 2665-2670.

(23) Walter, A.; Marz, A.; Schumacher, W.; Rosch, P.; Popp, J. *Lab on a chip* **2011**, *11*, 1013-1021.

(24) Lu, X.; Samuelson, D. R.; Xu, Y.; Zhang, H.; Wang, S.; Rasco, B. A.; Xu, J.; Konkel, M. E. *Analytical chemistry* **2013**, *85*, 2320-2327.

(25) Hassoun, M.; Ruger, J.; Kirchberger-Tolstik, T.; Schie, I. W.; Henkel, T.; Weber, K.; Cialla-May, D.; Krafft, C.; Popp, J. *Analytical and bioanalytical chemistry* **2017**.

(26) Schmitz, C. H.; Rowat, A. C.; Koster, S.; Weitz, D. A. *Lab on a chip* **2009**, *9*, 44-49.

(27) Raval, G. N.; Parekh, L. J.; Patel, D. D.; Jha, F. P.; Sainger, R. N.; Patel, P. S. *Indian journal of clinical biochemistry : IJCB* **2004**, *19*, 60-71.

(28) McMillan, K. S.; McCluskey, A. G.; Sorensen, A.; Boyd, M.; Zagnoni, M. *The Analyst* **2016**, *141*, 100-110.

(29) Collins, D. J.; Neild, A.; deMello, A.; Liu, A. Q.; Ai, Y. *Lab on a chip* **2015**, *15*, 3439-3459.

(30) Eilers, P. H. *Analytical chemistry* **2004**, *76*, 404-411.

(31) Leng, W.; Vikesland, P. J. *Langmuir : the ACS journal of surfaces and colloids* **2014**, *30*, 8342-8349.

(32) Smith, A. L. *Spectrochim Acta* **1960**, *16*, 87-105.

(33) Cai, D.; Neyer, A.; Kuckuk, R.; Heise, H. M. *Journal of Molecular Structure* **2010**, *976*, 274-281.

(34) Jayes, L.; Hard, A. P.; Sene, C.; Parker, S. F.; Jayasooriya, U. A. *Analytical chemistry* **2003**, *75*, 742-746.

(35) Wei, H.; Willner, M. R.; Marr, L. C.; Vikesland, P. J. *The Analyst* **2016**, *141*, 5159-5169.

(36) Willner, M. R.: Zenodo, 2017.

(37) Burgess, A.; Vigneron, S.; Brioudes, E.; Labbe, J. C.; Lorca, T.; Castro, A. *Proceedings of the National Academy of Sciences of the United States of America* **2010**, *107*, 12564-12569.

(38) McCloy, R. A.; Rogers, S.; Caldon, C. E.; Lorca, T.; Castro, A.; Burgess, A. *Cell Cycle* **2014**, *13*, 1400-1412.

(39) Haiss, W.; Thanh, N. T. K.; Aveyard, J.; Fernig, D. G. *Analytical chemistry* **2007**, *79*, 4215-4221.